Angular Fluctuations of a Multicomponent Order Describe the Pseudogap of \(YBa_2Cu_3O_{6+x}\)

Angular fluctuations of a multi-component order describe the pseudogap regime of the cuprate superconductors

Lauren E. Hayward,[1] David G. Hawthorn,[1] Roger G. Melko,[1,2] and Subir Sachdev[3]

[1]*Department of Physics and Astronomy, University of Waterloo, Ontario, N2L 3G1, Canada*

[2]*Perimeter Institute for Theoretical Physics, Waterloo, Ontario N2L 2Y5, Canada*

[3]*Department of Physics, Harvard University, Cambridge MA 02138*

The hole-doped cuprate high temperature superconductors enter the pseudogap regime as their superconducting critical temperature, T_c, falls with decreasing hole density. Experiments have probed this regime for over two decades, but we argue that decisive new information has emerged from recent X-ray scattering experiments [1–3]. The experiments observe incommensurate charge density wave fluctuations whose strength rises gradually over a wide temperature range above T_c, but then decreases as the temperature is lowered below T_c. We propose a theory in which the superconducting and charge-density wave orders exhibit angular fluctuations in a 6-dimensional space. The theory provides a natural quantitative fit to the X-ray data, and is consistent with other observed characteristics of the pseudogap.

The X-ray scattering intensity [4] of $YBa_2Cu_3O_{6.67}$ at the incommensurate wavevectors $\boldsymbol{Q}_x \approx (0.31, 0)$ or $\boldsymbol{Q}_y \approx (0, 0.31)$, shown in Fig. 1, increases gradually below $T \approx 200$K in a concave-upward shape until just above $T_c = 60$K. One possibility is that this represents an order parameter of a broken symmetry, and the correlation length is arrested at a finite value by disorder; however, such order parameters invariably have a concave-downward shape. The temperature range is also too wide to represent the precursor critical fluctuations of an ordering transition. Indeed, there is no ordering transition below T_c, and, remarkably, the scattering intensity decreases below T_c at a rate similar to that of the rate of increase above T_c.

Instead, the increase in intensity between 200K and 60K is reminiscent of the classic measurement by Keimer *et al.* [5], who observed a gradual increase in the neutron scattering

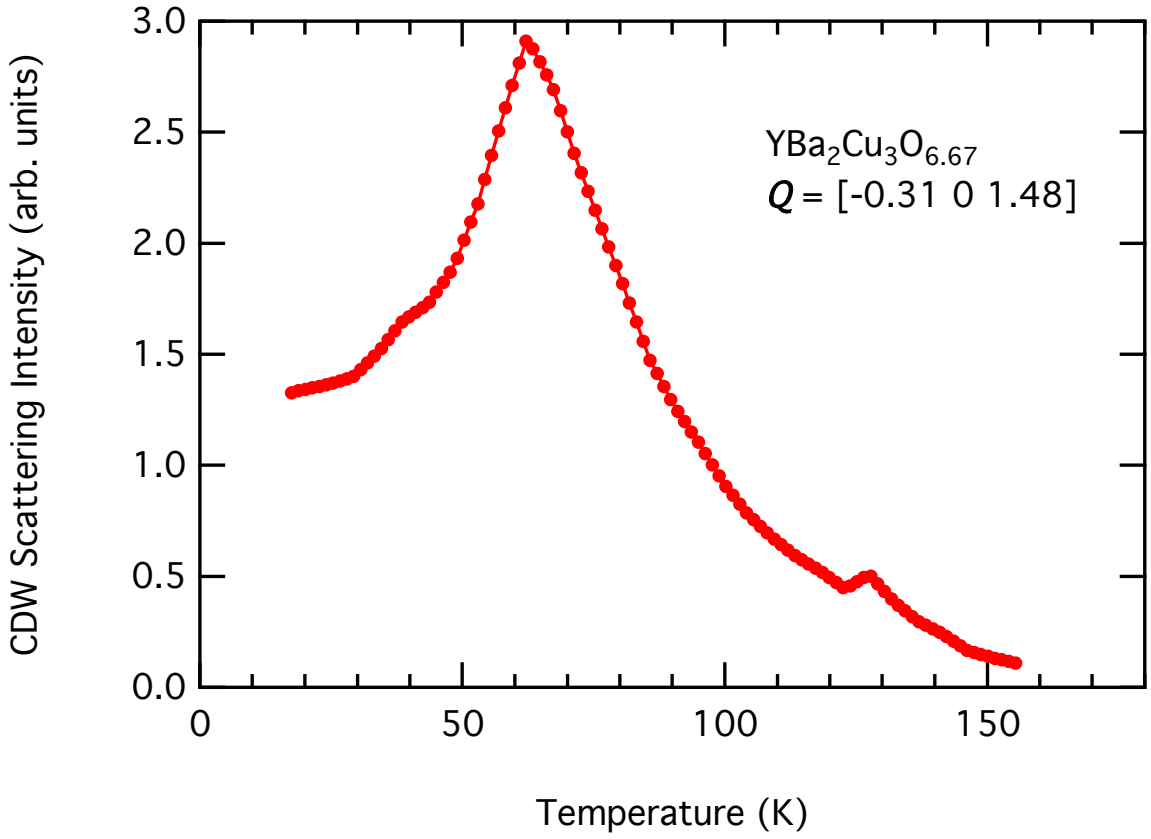

FIG. 1: The temperature dependence of the CDW scattering intensity at $\mathbf{Q}$ = [-0.31 0 1.48] in $YBa_2Cu_3O_{6.67}$ measured by resonant x-ray scattering in Ref. [4]. This sample has $T_c \approx 65.5$K.

intensity at the antiferromagnetic wavevector in the insulating antiferromagnet La_2CuO_4 between 550K and 350K [6]. This increase was explained by the classical thermal, angular fluctuations of the 3-component antiferromagnetic order parameter in $d = 2$ spatial dimensions [7]. Indeed, this is a special case of a general result of Polyakov [8] who showed that order parameters with $N \geq 3$ components are dominated by angular fluctuations in $d = 2$; here, we will exploit the $N = 6$ case to describe X-ray scattering in the pseudogap of $YBa_2Cu_3O_{6.67}$.

The observed decrease in charge order with decreasing T in $YBa_2Cu_3O_{6.67}$ at low T was predicted in Ref. [9], using a Landau theory framework [10] to describe competition between superconductivity and charge density wave order [11, 12]. Here we will extend the theory to a much wider regime of temperatures. The Landau theory introduces a complex field $\Psi(\boldsymbol{r})$ to represent the superconductivity, and two complex fields $\Phi_{x,y}(\boldsymbol{r})$ to represent the charge order. The latter can represent modulations at the wavevectors $\boldsymbol{Q}_{x,y}$ in not only the site

charge density, but also modulations in bond variables associated with a pair of sites [12, 13]; nevertheless, we will refer to it simply as "charge" order. The free energy is restricted by 3 distinct U(1) symmetries: charge conservation, translations in x, and translations in y, which rotate the phases of Ψ, Φ_x, and Φ_y respectively. There are also the discrete symmetries of time-reversal and the square lattice point group, and these lead to the following form of the Landau free energy density (we ignore possible anisotropies in the spatial derivative terms):

$$\begin{aligned} F \;=\; & |\nabla\Psi|^2 + s_1|\Psi|^2 + u_1|\Psi|^4 + |\nabla\Phi_x|^2 + |\nabla\Phi_y|^2 + s_2\left(|\Phi_x|^2 + |\Phi_y|^2\right) \\ & + u_2\left(|\Phi_x|^2 + |\Phi_y|^2\right)^2 + w\left(|\Phi_x|^4 + |\Phi_y|^4\right) + v|\Psi|^2\left(|\Phi_x|^2 + |\Phi_y|^2\right) \end{aligned} \tag{1}$$

The competing order effect arises from the $v > 0$ term, which demands that $|\Phi_{x,y}|$ increase when $|\Psi|$ decreases, and vice-versa. The earlier analysis [9] was perturbative in v, and consequently applies only in a narrow window around T_c.

We develop a theory which is non-perturbative in v by assuming that the origin of the 6-dimensional space defined by (Ψ, Φ_x, Φ_y) only has high energy states, and so should be excluded; see Fig. 2. In other words, we assume it is always preferable for the electronic Fermi surface to locally acquire some type of order. For each radial direction in this 6-dimensional space, we can label the optimal state by a unit vector n_α ($\alpha = 1 \ldots 6$) with $\Psi \propto n_1 + in_2$, $\Phi_x \propto n_3 + in_4$, and $\Phi_y \propto n_5 + in_6$. Our primary physical assumption is that amplitude fluctuations along the radial direction can be neglected, and that we can focus solely on the angular fluctuations; no assumptions of an approximate O(6) symmetry are made a priori. So we introduce a partition function for angular fluctuations of n_α, with all terms allowed by the symmetries noted earlier:

$$\begin{aligned} \mathcal{Z} \;=\; & \int \mathcal{D}n_\alpha(\boldsymbol{r})\,\delta\left(\sum_{\alpha=1}^{6} n_\alpha^2(\boldsymbol{r}) - 1\right) \exp\left(-\frac{\rho_s}{2T}\int d^2r \left[\sum_{\alpha=1}^{2}(\nabla n_\alpha)^2 + \lambda\sum_{\alpha=3}^{6}(\nabla n_\alpha)^2\right.\right. \\ & \left.\left. + g\sum_{\alpha=3}^{6} n_\alpha^2 + w\left[\left(n_3^2 + n_4^2\right)^2 + \left(n_5^2 + n_6^2\right)^2\right]\right]\right). \end{aligned} \tag{2}$$

The couplings ρ_s and $\rho_s\lambda$ are the helicity moduli for spatial variations of the superconducting and charge orders respectively. The coupling g measure the relative energetic cost of ordering between the superconducting and charge order directions; this is most relevant term which breaks the O(6) symmetry present for $\lambda = 1$, $g = 0$, $w = 0$ to O(4)×O(2) symmetry. Finally w imposes the square lattice point group symmetry on the charge order: for $w < 0$ the charge is uni-directional with only one of Φ_x or Φ_y non-zero, while for $w > 0$ the charge

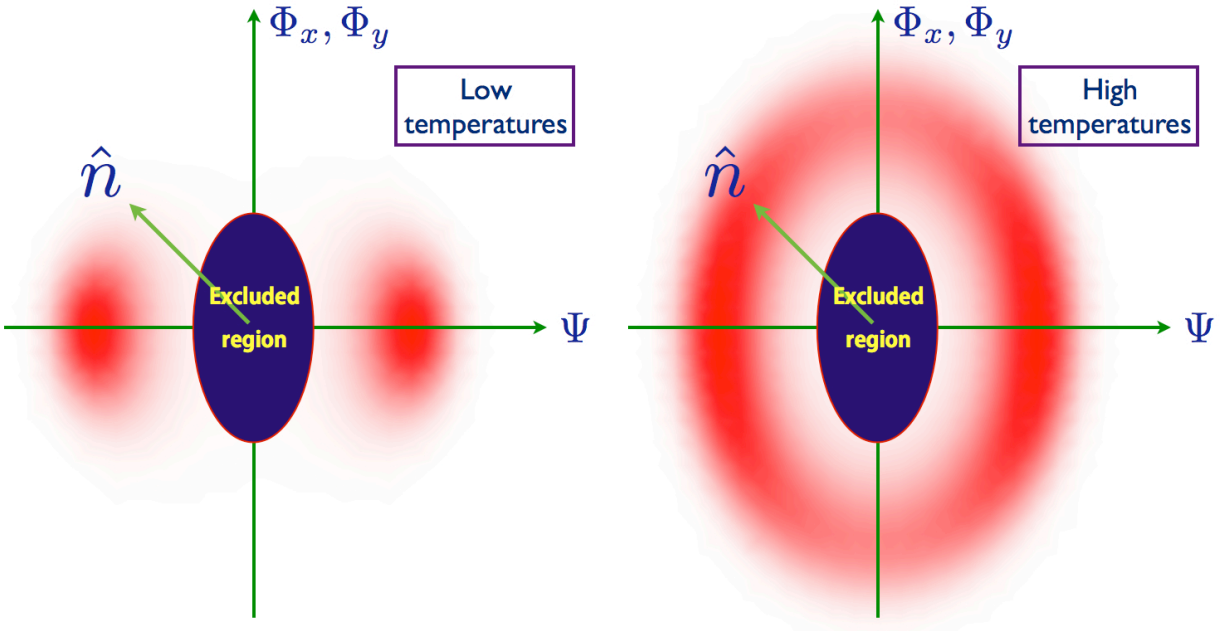

FIG. 2: Schematic of the structure of fluctuations of $\mathcal{Z}$ in a 6-dimensional space representing the complex superconducting order, Ψ, and the complex charge orders $\Phi_{x,y}$. At high T, all angles are explored, while at low T below T_c, for $g > 0$, the order lies mainly along the equator in the plane representing Ψ.

ordering is bi-directional. The final symmetry of $\mathcal{Z}$ is $O(2)\times O(2)\times O(2)\rtimes\mathbb{Z}_2$, where the 3 O(2)'s are enlarged by discrete symmetries from the 3 U(1)'s noted earlier, and the $\mathbb{Z}_2$ represents the 90° spatial rotation symmetry, whose spontaneous breaking is measured by the Ising-nematic order [14] $m = |\Phi_x|^2 - |\Phi_y|^2$.

The enhanced symmetries of $\mathcal{Z}$ at $\lambda = 1$, $g = 0$, $w = 0$ include two SO(4) rotation symmetries between d-wave superconductivity and incommensurate d-wave bond order (but the latter with $\boldsymbol{Q}$'s along the $(1, \pm 1)$ directions) that emerge at low energies in the vicinity of a generic quantum critical point for the onset of antiferromagnetism in a metal [15]; a non-linear sigma model of this theory was developed by Efetov *et al.* [16] and applied to the phase diagram in a magnetic field [17]. It was also argued [13] that these symmetries can be viewed as remnants of the SU(2) pseudospin gauge invariances of Mott insulators [18–20], when extended to metals with a strong local antiferromagnetic exchange coupling. And we also note the similarity to the SO(5) non-linear sigma model of competing orders [21], which has antiferromagnetism, rather than charge order, competing with superconductivity.

A crucial feature of our analysis of $\mathcal{Z}$ is that the couplings ρ_s, g, λ, and w are assumed to

be T-independent. The dependence on absolute temperature arises only from the Boltzmann $1/T$ factor in $\mathcal{Z}$, and this strongly constrains our fits to the experimental data. This feature ensures our restriction to angular and classical fluctuations in the order parameter space.

We computed the properties of $\mathcal{Z}$ using a classical Monte Carlo simulation. This was performed using the Wolff cluster algorithm, after the continuum theory was discretized on a square lattice of spacing a. This lattice is not related to the underlying square lattice of Cu atoms in the cuprates; instead, it is just a convenient ultraviolet regularization of the continuum theory, and we don't expect our results to be sensitive to the particular regularization chosen. All length scales in our results will be proportional to the value of a, and the value of a has to be ultimately determined by matching one of them to experiments. We performed simulations on lattice sizes up to 72×72, and were able to control all finite size effects.

We also performed a $1/N$ expansion on a generalized model with N components of n_α, as described in the Appendix. It was found to be quite accurate for the charge order correlations, but does not properly describe the superconducting correlations near T_c and below.

Our Monte Carlo results for the charge order correlations are shown in Fig. 3. We computed the structure factor

$$S_{\Phi_x}(p) = \int d^2r \sum_{\alpha=3}^{4} \langle n_\alpha(\boldsymbol{r}) n_\alpha(0)\rangle \, e^{i\boldsymbol{p}\cdot\boldsymbol{r}} \tag{3}$$

and show the values of $S_{\Phi_x} \equiv S_{\Phi_x}(p=0)$ for a variety of parameters. At high T, we have regime of increasing S_{Φ_x} with decreasing T, as the correlation length of both the superconductivity and charge order increases, and the order parameter fluctuates over all 6 directions (see Fig. 2). At low T, there is onset of superconducting order, and S_{Φ_x} decreases with decreasing T, as the order parameter becomes confined to the Ψ plane. In Fig. 3, we fit the position of the peak in S_{Φ_x} by choosing the value of ρ_s, and adjusted the vertical scale so that the peak height also coincides. Note that we are not allowed to shift the horizontal axis, as T is predetermined. The peak width and shape is *not* adjustable and is determined by the theory; so it can be used to fix the values of the dimensionless parameters ga^2, wa^2, and λ. It is evident that the theory naturally reproduces the experimental curve, including the rate of decrease of charge order on both sides of the peak, for a range of parameter values. Another view of S_{Φ_x} is in Fig. 4, where we present results of the $1/N$ expansion.

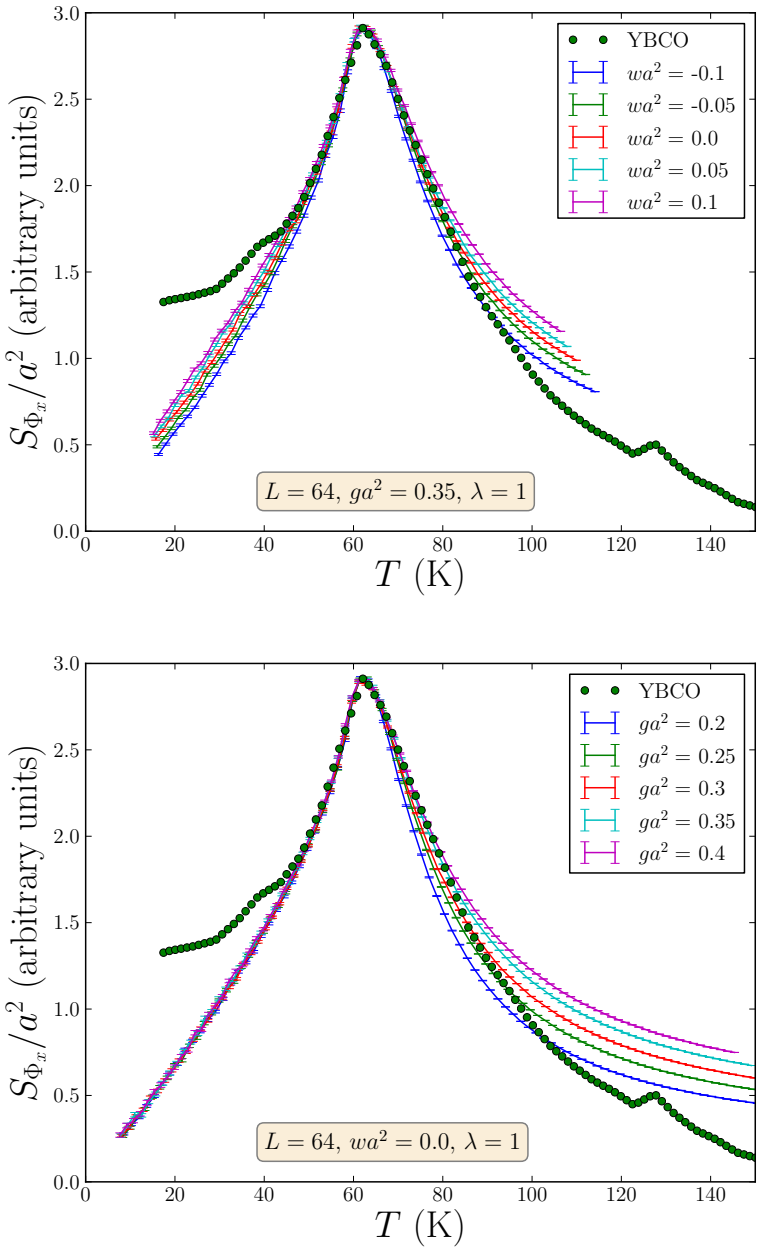

FIG. 3: Comparison of the X-ray data to Monte Carlo simulations of $\mathcal{Z}$. For each set of values of ga^2, wa^2 and λ, there were 2 fitting parameters. The value of ρ_s was determined for each data set so that the peak positions match: this is equivalent to a rescaling (but not shifting) of the T-axis. The peak width or shape is *not* adjustable. For $ga^2 = 0.30$ and $wa^2 = 0.0$ we have $\rho_s = 160$K. The height was also rescaled to make the peak heights match.

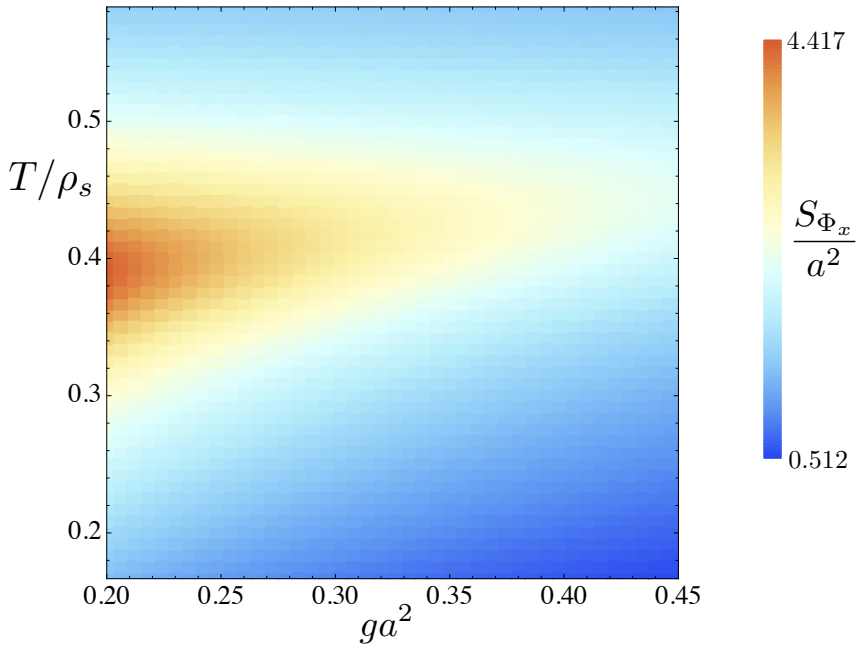

FIG. 4: Density plot of S_{Φ_x} as a function of ga^2 and T/ρ_s, for $\lambda = 1$ and $wa^2 = 0.1$ at order $1/N$ in the large N expansion.

Note that there are differences between the experiment and theory in Fig. 3, both at very low and very high T. However, the deviations are in the expected directions. At low T, in the present classical theory, S_{Φ_x} vanishes as $T \to 0$; however, quantum fluctuations will increase S_{Φ_x}, possibly accounting for the deviation. At high T, we expect the bare value of the stiffness ρ_s to decrease, in contrast to the T-independent ρ_s in our theory: this should decrease S_{Φ_x} as needed.

Next, we examined the superconducting correlations by measuring the associated helicity modulus. As shown in Fig. 5, this allows us to determine T_c by comparing against the expected universal jump [22]. We find a T_c below the peak in S_{Φ_x}. This is consistent with the arguments in Ref. [9], which predicted a monotonic decrease in charge order through T_c: evidently their computations only apply in a narrow window about T_c. We note that we have not accounted to inter-layer couplings in our two-dimensional theory, and this can raise T_c to a position nearer the peak, as in Fig. 1.

One of the fundamental aspects of our theory is that the *same* set of parameters used above to describe X-ray scattering experiments, also predict the strength of superconducting fluctuations above T_c. The latter are detectable in diamagnetism measurements, and

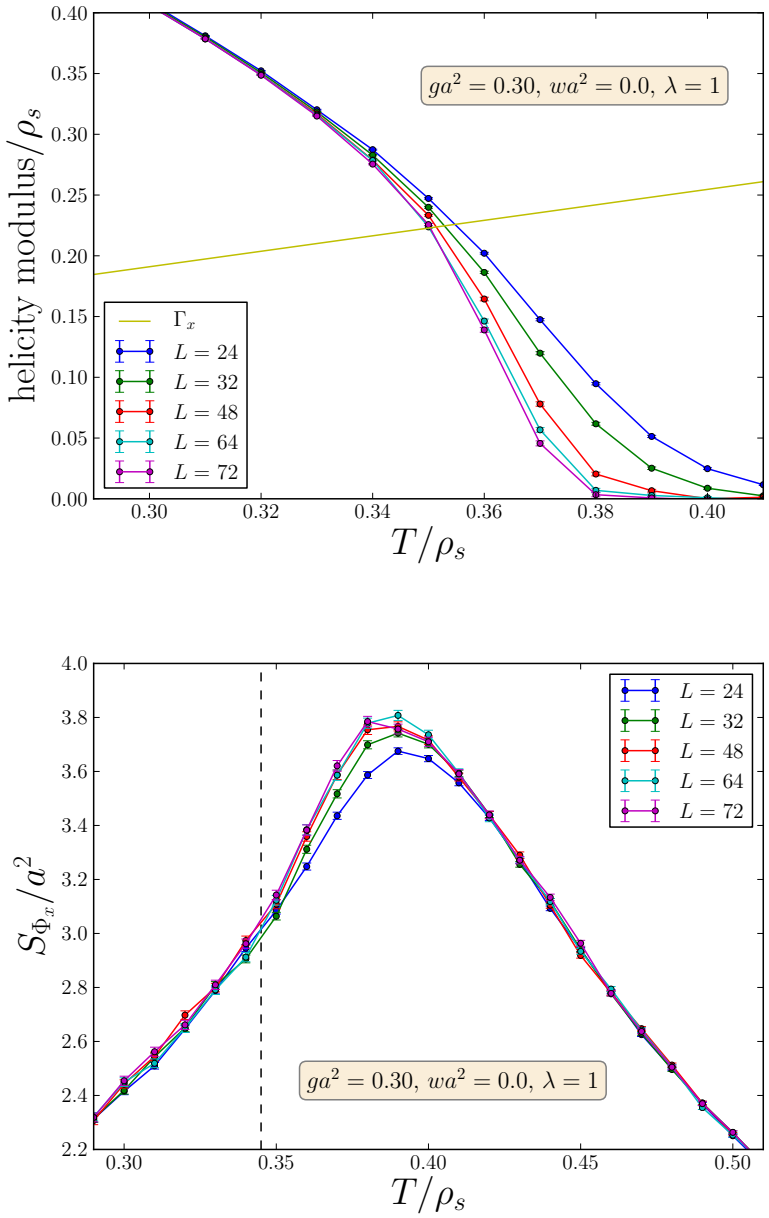

FIG. 5: Top: Monte Carlo results for the helicity modulus, measured in the x-direction. Note that ρ_s is the helicity modulus at $T = 0$. We also plot $\Gamma_x = (2/\pi)T/\rho_s$, and use the relation helicity modulus $= (2/\pi)T_c$ [22] to determine the Kosterlitz-Thouless temperature for each system size L. A finite-size scaling analysis estimates $T_c/\rho_s \approx 0.345$ for these parameters. Bottom: The structure factor, showing a peak at around $T/\rho_s = 0.39$. The Kosterlitz-Thouless temperature, T_c, is marked with a vertical dashed line. The prediction of Ref. [9] of increasing charge order with increasing temperature applies in the immediate vicinity of T_c, to the left of the peak.

indeed $YBa_2Cu_3O_{6+x}$ shows significant fluctuation diamagnetism [23, 24] over the range of temperatures that X-ray experiments measure charge order fluctuations. We compute the diamagnetic susceptibility in the $N = \infty$ theory in the Appendix; such a theory has effectively Gaussian superconducting fluctuations and is expected to apply only at T significantly above T_c. The observations [24] were found to be consistent with a Gaussian theory [25], with a T dependence of the superconducting coherence length, $\xi_{ab}(T)$, similar to that found in the Appendix. For a sharper comparison, we need to study the crossover into a vortex dominated regime [26–28]; its description requires Monte Carlo study in our theory, which is in progress. Making an absolute comparison of $\xi_{ab}(T)$ with our theory requires the value of a, which also determines the charge order correlation length. Eventually, with such a complete study, and more detailed measurements of charge order and superconducting correlations on the same sample, we expect to be able to more tightly constrain the values of ga^2, wa^2, λ, and a.

Other aspects of the charge order and superconducting fluctuations in the pseudogap regime are similar to those in previous discussions [13, 16, 29]. Charge order was originally observed around vortex cores [30, 31], indicating its competition with superconductivity. Bond order was observed [32] in tunneling microscopy at low T, in a disordered configuration frozen in by disorder. The charge order becomes long-ranged in high magnetic fields [33], and this is very likely connected to the observed quantum oscillations [34, 35]. The combination of fluctuating charge and superconducting order is expected to describe the photoemission observations [13, 29, 35]. The Kerr effect observations have also been linked to charge order [36].

Our discussion of the pseudogap here has been restricted to the regime of doping over which only charge order is observed at high fields [33]. At lower doping, there is a quantum critical point to the onset of magnetic order [37], and this indicates that our theory of the pseudogap will have to be extended to explicitly include magnetic fluctuations [38] at lower doping.

Acknowledgments. We thank A. Chubukov, A. Georges and A. Yacoby for useful discussions. This research was supported by the NSF under Grant DMR-1103860 and the Natural Sciences and Engineering Research Council of Canada. This research was also supported in part by Perimeter Institute for Theoretical Physics; research at Perimeter Institute is supported by the Government of Canada through Industry Canada and by the Province of

Ontario through the Ministry of Research and Innovation.

Appendix A: Large N expansion

We carried out the large N expansion of the partition function $\mathcal{Z}$ in Eq. (2) by generalizing it to a model with a N-component unit vector n_α in which the O(N) symmetry breaks down to O($N/3$)×O($N/3$)×O($N/3$)⋊$\mathbb{Z}_2$. The action for such a model is

$$\mathcal{S} = \frac{\rho_s}{2T}\int d^2r \left\{ \sum_{\alpha=1}^{N/3} (\nabla n_\alpha)^2 + \lambda \sum_{\alpha=N/3+1}^{N} (\nabla n_\alpha)^2 + g \sum_{\alpha=N/3+1}^{N} n_\alpha^2 + w\left[\left(\sum_{\alpha=N/3+1}^{2N/3} n_\alpha^2 \right)^2 + \left(\sum_{\alpha=2N/3+1}^{N} n_\alpha^2 \right)^2 \right] \right\}. \tag{A1}$$

The large N expansion proceeds by a standard method [39], and requires that

$$T = t/N, \tag{A2}$$

with t of order unity. We introduce an auxilliary field σ to impose the unit length constraint, and two fields $\phi_{x,y}$ which decouple the quartic terms. In this manner we obtain

$$\mathcal{S} = \frac{N\rho_s}{2t}\int d^2r \left\{ \sum_{\alpha=1}^{N/3} (\nabla n_\alpha)^2 + \lambda \sum_{\alpha=N/3+1}^{N} (\nabla n_\alpha)^2 + g \sum_{\alpha=N/3+1}^{N} n_\alpha^2 + i\sigma\left(\sum_{\alpha=1}^{N} n_\alpha^2 - 1 \right) + \frac{\phi_x^2+\phi_y^2}{4w} + i\phi_x \sum_{\alpha=N/3+1}^{2N/3} n_\alpha^2 + i\phi_y \sum_{\alpha=2N/3+1}^{N} n_\alpha^2 \right\}. \tag{A3}$$

In the $N=\infty$ limit, we can integrate out the n_α, and the auxilliary fields are all fixed at their saddle-point values $i\sigma = \overline{\sigma}$, $i\phi_{x,y} = \overline{\phi}_{x,y}$ which are determined by the saddle point equations

$$\begin{aligned} \frac{\rho_s}{t} &= \frac{1}{3}\int_{\boldsymbol{p}} \left[\frac{1}{p^2+\overline{\sigma}} + \frac{1}{\lambda p^2+\overline{\sigma}+g+\overline{\phi}_x} + \frac{1}{\lambda p^2+\overline{\sigma}+g+\overline{\phi}_y} \right] \\ \overline{\phi}_x &= \frac{2wt}{3\rho_s}\int_{\boldsymbol{p}} \frac{1}{\lambda p^2+\overline{\sigma}+g+\overline{\phi}_x} \\ \overline{\phi}_y &= \frac{2wt}{3\rho_s}\int_{\boldsymbol{p}} \frac{1}{\lambda p^2+\overline{\sigma}+g+\overline{\phi}_y} \end{aligned} \tag{A4}$$

where $\int_{\boldsymbol{p}} \equiv \int d^2p/(4\pi^2)$. The optimum solution minimizes the free energy density, which is given by

$$F = \frac{t}{6}\int_{\boldsymbol{p}} \ln\left[(p^2+\overline{\sigma})(\lambda p^2+\overline{\sigma}+g+\overline{\phi}_x)(\lambda p^2+\overline{\sigma}+g+\overline{\phi}_y) \right] - \frac{\rho_s\overline{\sigma}}{2} - \frac{\rho_s(\overline{\phi}_x^2+\overline{\phi}_y^2)}{8w} \tag{A5}$$

A solution with $\overline{\phi}_x \neq \overline{\phi}_y$ breaks Ising-nematic symmetry, and this happens at sufficiently low temperatures for $w < -g$ and $g > 0$, or for $w < 0$ and $g < 0$. The momentum-dependent structure factors of the Ψ, Φ_x, and Φ_y correlators are

$$\begin{aligned} S_\Psi(p) &= \frac{t/(3\rho_s)}{p^2 + \overline{\sigma}} \\ S_{\Phi_x}(p) &= \frac{t/(3\rho_s)}{\lambda p^2 + \overline{\sigma} + g + \overline{\phi}_x} \\ S_{\Phi_y}(p) &= \frac{t/(3\rho_s)}{\lambda p^2 + \overline{\sigma} + g + \overline{\phi}_y}. \end{aligned} \tag{A6}$$

For the $1/N$ corrections, we need to include fluctuations of $\sigma, \phi_{x,y}$ about their saddle point values. See Ref. [40] for details on a similar computation in a different context. The propagators of these fields are expressed in terms of 'polarization functions' which are given by

$$\begin{aligned} \Pi(p,\overline{\sigma}) &= \frac{1}{3}\int_{\boldsymbol{q}} \Bigg[\frac{1}{(q^2+\overline{\sigma})((\boldsymbol{p}+\boldsymbol{q})^2+\overline{\sigma})} + \frac{1}{(\lambda q^2 + \overline{\sigma} + g + \overline{\phi}_x)(\lambda(\boldsymbol{p}+\boldsymbol{q})^2 + \overline{\sigma} + g + \overline{\phi}_x)} \\ &\qquad + \frac{1}{(\lambda q^2 + \overline{\sigma} + g + \overline{\phi}_y)(\lambda(\boldsymbol{p}+\boldsymbol{q})^2 + \overline{\sigma} + g + \overline{\phi}_y)} \Bigg] \\ \Pi_x(p,\overline{\sigma}) &= \frac{\rho_s}{2wt} + \frac{1}{3}\int_{\boldsymbol{q}} \frac{1}{(\lambda q^2 + \overline{\sigma} + g + \overline{\phi}_x)(\lambda(\boldsymbol{p}+\boldsymbol{q})^2 + \overline{\sigma} + g + \overline{\phi}_x)} \\ \Pi_y(p,\overline{\sigma}) &= \frac{\rho_s}{2wt} + \frac{1}{3}\int_{\boldsymbol{q}} \frac{1}{(\lambda q^2 + \overline{\sigma} + g + \overline{\phi}_y)(\lambda(\boldsymbol{p}+\boldsymbol{q})^2 + \overline{\sigma} + g + \overline{\phi}_y)} \end{aligned} \tag{A7}$$

Then after including self-energy corrections in the n_α propagators, we obtain the $1/N$ cor-

rections to Eq. (A6):

$$
\begin{aligned}
\frac{t}{3\rho_s}S^{-1}_{\Psi}(p) &= p^2+\overline{\sigma}+\frac{1}{N}\frac{1}{\Pi(0,\overline{\sigma})}\int_{\boldsymbol{q}}\frac{1}{\Pi(q,\overline{\sigma})}\left[\frac{d\Pi(q,\overline{\sigma})}{d\overline{\sigma}}+\frac{2\Pi(0,\overline{\sigma})}{((\boldsymbol{p}+\boldsymbol{q})^2+\overline{\sigma})}\right]\\
&\quad+\frac{1}{N}\frac{1}{\Pi(0,\overline{\sigma})}\int_{\boldsymbol{q}}\frac{1}{\Pi_x(q,\overline{\sigma})}\frac{d\Pi_x(q,\overline{\sigma})}{d\overline{\sigma}}+\frac{1}{N}\frac{1}{\Pi(0,\overline{\sigma})}\int_{\boldsymbol{q}}\frac{1}{\Pi_y(q,\overline{\sigma})}\frac{d\Pi_y(q,\overline{\sigma})}{d\overline{\sigma}}\\
\frac{t}{3\rho_s}S^{-1}_{\Phi_x}(p) &= \lambda p^2+\overline{\sigma}+g+\overline{\phi}_x+\frac{1}{N}\frac{1}{\Pi(0,\overline{\sigma})}\int_{\boldsymbol{q}}\frac{1}{\Pi(q,\overline{\sigma})}\left[\frac{d\Pi(q,\overline{\sigma})}{d\overline{\sigma}}+\frac{2\Pi(0,\overline{\sigma})}{(\lambda(\boldsymbol{p}+\boldsymbol{q})^2+\overline{\sigma}+g+\overline{\phi}_x)}\right]\\
&\quad+\frac{1}{N}\frac{1}{\Pi(0,\overline{\sigma})}\int_{\boldsymbol{q}}\frac{1}{\Pi_x(q,\overline{\sigma})}\frac{d\Pi_x(q,\overline{\sigma})}{d\overline{\sigma}}+\frac{1}{N}\frac{1}{\Pi(0,\overline{\sigma})}\int_{\boldsymbol{q}}\frac{1}{\Pi_y(q,\overline{\sigma})}\frac{d\Pi_y(q,\overline{\sigma})}{d\overline{\sigma}}\\
&\quad+\frac{1}{N}\frac{1}{\Pi_x(0,\overline{\sigma})}\int_{\boldsymbol{q}}\frac{1}{\Pi_x(q,\overline{\sigma})}\left[\frac{d\Pi_x(q,\overline{\sigma})}{d\overline{\sigma}}+\frac{2\Pi_x(0,\overline{\sigma})}{(\lambda(\boldsymbol{p}+\boldsymbol{q})^2+\overline{\sigma}+g+\overline{\phi}_x)}\right]\\
&\quad+\frac{1}{N}\frac{1}{\Pi_x(0,\overline{\sigma})}\int_{\boldsymbol{q}}\frac{1}{\Pi(q,\overline{\sigma})}\frac{d\Pi_x(q,\overline{\sigma})}{d\overline{\sigma}}\\
\frac{t}{3\rho_s}S^{-1}_{\Phi_y}(p) &= \lambda p^2+\overline{\sigma}+g+\overline{\phi}_y+\frac{1}{N}\frac{1}{\Pi(0,\overline{\sigma})}\int_{\boldsymbol{q}}\frac{1}{\Pi(q,\overline{\sigma})}\left[\frac{d\Pi(q,\overline{\sigma})}{d\overline{\sigma}}+\frac{2\Pi(0,\overline{\sigma})}{(\lambda(\boldsymbol{p}+\boldsymbol{q})^2+\overline{\sigma}+g+\overline{\phi}_y)}\right]\\
&\quad+\frac{1}{N}\frac{1}{\Pi(0,\overline{\sigma})}\int_{\boldsymbol{q}}\frac{1}{\Pi_x(q,\overline{\sigma})}\frac{d\Pi_x(q,\overline{\sigma})}{d\overline{\sigma}}+\frac{1}{N}\frac{1}{\Pi(0,\overline{\sigma})}\int_{\boldsymbol{q}}\frac{1}{\Pi_y(q,\overline{\sigma})}\frac{d\Pi_y(q,\overline{\sigma})}{d\overline{\sigma}}\\
&\quad+\frac{1}{N}\frac{1}{\Pi_y(0,\overline{\sigma})}\int_{\boldsymbol{q}}\frac{1}{\Pi_y(q,\overline{\sigma})}\left[\frac{d\Pi_y(q,\overline{\sigma})}{d\overline{\sigma}}+\frac{2\Pi_y(0,\overline{\sigma})}{(\lambda(\boldsymbol{p}+\boldsymbol{q})^2+\overline{\sigma}+g+\overline{\phi}_y)}\right]\\
&\quad+\frac{1}{N}\frac{1}{\Pi_y(0,\overline{\sigma})}\int_{\boldsymbol{q}}\frac{1}{\Pi(q,\overline{\sigma})}\frac{d\Pi_y(q,\overline{\sigma})}{d\overline{\sigma}}
\end{aligned}
\tag{A8}
$$

We evaluated these expressions numerically after regulating the theory on a square lattice with lattice spacing a. Operationally, this means that we perform the replacement $p^2 \to (4-2\cos(p_x a)-2\cos(p_y a))/a^2$ in all propagators, and the $p_{x,y}$ integrals extend from $-\pi/a$ to π/a. We show our results for the equal-time structure factor of the charge order correlations $S_{\Phi_x} \equiv S_{\Phi_x}(p=0)$ in Fig. 6. For the parameters for which results are shown, we found good convergence upon replacing each integral by a discrete sum over 200 points. It is evident that the $1/N$ expansion is quite accurate, except near the peaks.

1. Ising-nematic correlations

We also computed the structure factor of the Ising-nematic order in the phase where Ising-nematic order is preserved. The Ising-nematic order is $m = \sum_{\alpha=N/3+1}^{2N/3} n_\alpha^2 - \sum_{\alpha=2N/3+1}^{N} n_\alpha^2$ and S_m is its two-point correlator. We compute this by including a source J in the action $\mathcal{S} \to \mathcal{S} + \int d^2r\, J\, m$. Then, after shifting the auxiliary fields and integrating out the n_α, we

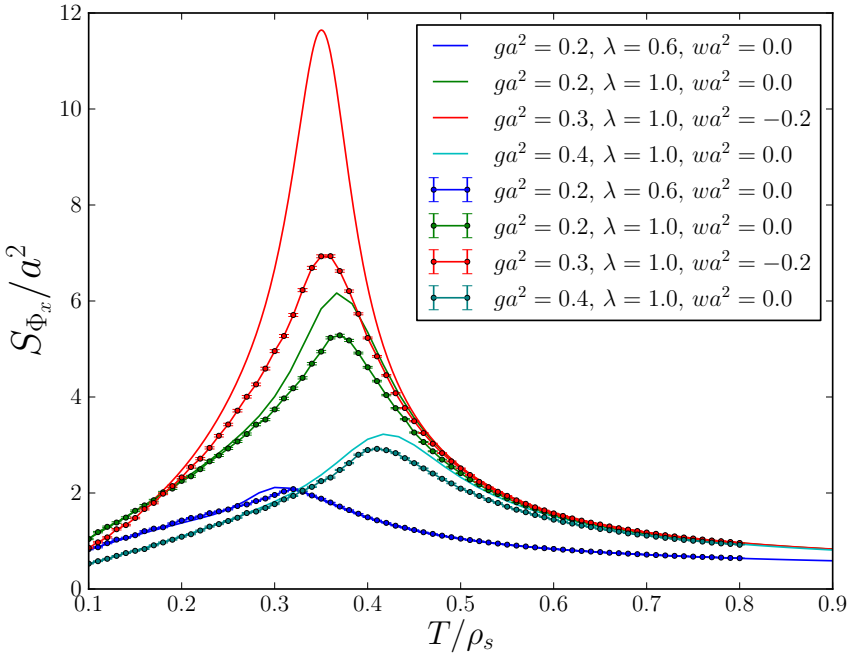

FIG. 6: Comparison of the charge order structure factor as obtained from the large N expansion at order $1/N$, with the computations of the Monte Carlo for the same parameters, and size $L = 32$. Large N calculations are solid lines, and Monte Carlo data is plotted as circles with statistical error bars.

find that the effective action for the auxiliary fields maps via

$$\mathcal{S}[\sigma, \phi_x, \phi_y] \to \mathcal{S}[\sigma, \phi_x, \phi_y] + \frac{i}{2w} J\left(\phi_x - \phi_y\right) - \frac{t}{N\rho_s w} J^2 \tag{A9}$$

By taking functional derivatives with respect to J, and then setting $J = 0$, we can now relate the Ising structure factor to the 2-point correlation of the auxiliary fields:

$$S_m(p) = \frac{2t}{N\rho_s w} - \frac{1}{4w^2} \int d^2r\, e^{i\boldsymbol{p}\cdot\boldsymbol{r}} \left\langle \left(\phi_x(\boldsymbol{r}) - \phi_y(\boldsymbol{r})\right)\left(\phi_x(0) - \phi_y(0)\right)\right\rangle \tag{A10}$$

At leading order in the $1/N$ expansion we can evaluate the correlator using the polarization functions in Eq. (A7); because we are in the Ising-symmetric phase, $\Pi_x = \Pi_y$, and

$$NS_m(p) = \frac{2t}{w\rho_s} - \frac{1}{w^2\Pi_x(p, \overline{\sigma})} = \frac{4(t/\rho_s)^2 P(p)}{3 + 2w(t/\rho_s)P(p)} \tag{A11}$$

where

$$P(p) = \int_{\boldsymbol{q}} \frac{1}{(\lambda q^2 + \overline{\sigma} + g + \overline{\phi}_x)(\lambda(\boldsymbol{p}+\boldsymbol{q})^2 + \overline{\sigma} + g + \overline{\phi}_x)} \tag{A12}$$

We show the T dependence of $S_m \equiv S_m(p = 0)$ in Fig. 7 for a particular set of couplings.

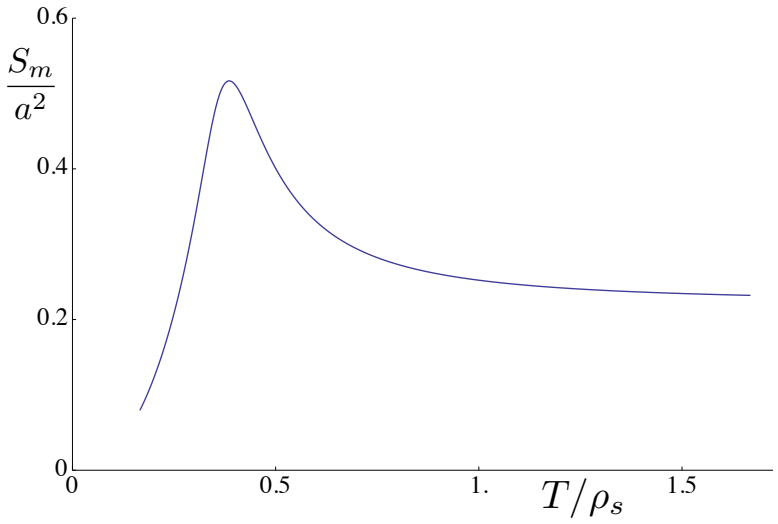

FIG. 7: Ising-nematic structure factor, as computed in the $N = \infty$ theory for $ga^2 = 0.3$, $\lambda = 1$ and $wa^2 = -0.2$. The corresponding charge ordering structure factor for these parameters is shown in Fig. 6.

2. Diamagnetic susceptibility

We now compute the linear response to a magnetic field applied perpendicular to the layer in the $N = \infty$ theory. We assume that the field only has an orbital coupling to the superconducting order. Here, we will carry out the computation explicitly with lattice regularization, on a square lattice of spacing a, because we want to keep all expressions properly gauge-invariant.

At $N = \infty$ we can set $i\sigma = \overline{\sigma}$, and just treat the $\alpha = 1, 2$ components of n_α as Gaussian fields. So we define the complex superconducting order by $\Psi = (n_1 + in_2)/\sqrt{2t/(N\rho_s)}$. Then the part of the action that detects the presence of the magnetic field is

$$\mathcal{S}_\Psi = -\sum_{\langle ij \rangle} \left(\Psi_i^* \Psi_j e^{iA_{ij}} + \text{c.c} \right) + \sum_i (4 + \overline{\sigma} a^2) |\Psi_i|^2 \tag{A13}$$

where A_{ij} is the Peierls phase from the applied field. The paramagnetic current is

$$J_i(\boldsymbol{q}) = \frac{2}{a} \int \frac{d^2k}{4\pi^2} \Psi^*(\boldsymbol{k} + \boldsymbol{q}/2) \Psi(\boldsymbol{k} - \boldsymbol{q}/2) \sin(k_i a) \tag{A14}$$

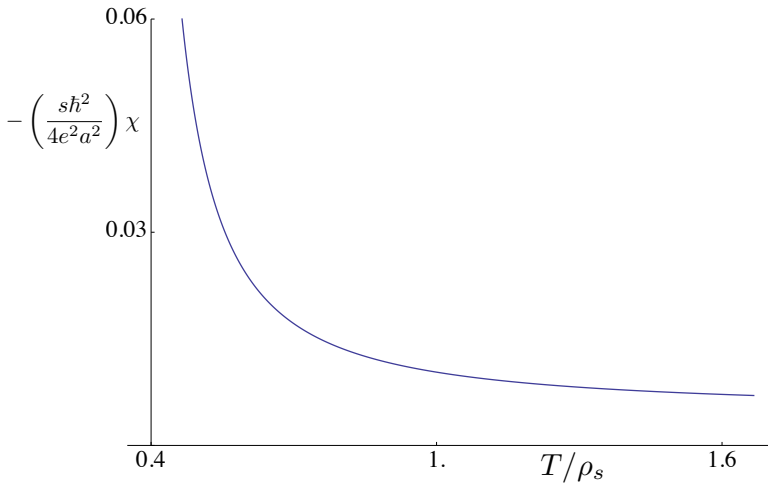

FIG. 8: Diamagnetic susceptibility for the same set of parameters as in Fig. 7.

So the 2-point current correlator, including the diamagnetic contribution, is

$$\begin{aligned} K_{ij}(\boldsymbol{q}) &= \langle J_i(\boldsymbol{q}) J_j(-\boldsymbol{q})\rangle \\ &= \frac{1}{a^2}\int \frac{d^2k}{4\pi^2} \frac{4\sin(k_i a)\sin(k_j a)}{((4-2\cos((k_x+q_x/2)a)-2\cos((k_y+q_y/2)a))/a^2+\overline{\sigma})} \\ &\qquad \times \frac{1}{((4-2\cos((k_x-q_x/2)a)-2\cos((k_y-q_y/2)a))/a^2+\overline{\sigma})} \\ &\quad - \delta_{ij}\int \frac{d^2k}{4\pi^2} \frac{2\cos(k_x a)}{((4-2\cos(k_x a)-2\cos(k_y a))/a^2+\overline{\sigma})} \end{aligned} \tag{A15}$$

This vanishes at $\boldsymbol{q}=0$ as expected by gauge invariance. For small $\boldsymbol{q}$ we obtain

$$K_{ij}(\boldsymbol{q}) = -(q^2\delta_{ij}-q_i q_j)\frac{1}{a^4}\int \frac{d^2k}{4\pi^2} \frac{8\sin^2(k_x a)\sin^2(k_y a)}{((4-2\cos(k_x a)-2\cos(k_y a))/a^2+\overline{\sigma})^4} \tag{A16}$$

For small $\overline{\sigma}$, the integral can be evaluated near $\boldsymbol{k}=0$, and we obtain

$$K_{ij}(\boldsymbol{q}) = -\frac{(q^2\delta_{ij}-q_i q_j)}{12\pi\overline{\sigma}} \tag{A17}$$

Restoring physical units, this implies that the magnetic susceptibility is

$$\chi = -\frac{1}{s}\left(\frac{2e}{\hbar}\right)^2 \frac{k_B T}{12\pi\overline{\sigma}} \tag{A18}$$

where s is the interlayer spacing. This agrees precisely with the standard result [25] in Eq. (1) of Ref. [24], after we observe from Eq. (A13) that $\overline{\sigma}$ is equal to $\xi_{ab}^{-2}(T)$, where $\xi_{ab}(T)$ is the superconducting coherence length.

We plot the T dependence of χ in Fig. 8 for the same set of parameters used in Fig. 7. We have only shown higher T values because the large N theory, which is effectively a Gaussian

theory, is not reliable close to the superconducting T_c. Note that the T dependence of χ, and hence also that of $\xi_{ab}(T)$, is similar to that in the observations [24].

---

[1] G. Ghiringhelli, M. Le Tacon, M. Minola, S. Blanco-Canosa, C. Mazzoli, N. B. Brookes, G. M. De Luca, A. Frano, D. G. Hawthorn, F. He, T. Loew, M. Moretti Sala, D. C. Peets, M. Salluzzo, E. Schierle, R. Sutarto, G. A. Sawatzky, E. Weschke, B. Keimer, and L. Braicovich, "Long-range incommensurate charge fluctuations in (Y,Nd)$Ba_2Cu_3O_{6+x}$," Science **337**, 821 (2012).

[2] J. Chang, E. Blackburn, A. T. Holmes, N. B. Christensen, J. Larsen, J. Mesot, Ruixing Liang, D. A. Bonn, W. N. Hardy, A. Watenphul, M. v. Zimmermann, E. M. Forgan, and S. M. Hayden, "Direct observation of competition between superconductivity and charge density wave order in $YBa_2Cu_3O_{6.67}$," Nature Phys. **8**, 871 (2012).

[3] A. J. Achkar, R. Sutarto, X. Mao, F. He, A. Frano, S. Blanco-Canosa, M. Le Tacon, G. Ghiringhelli, L. Braicovich, M. Minola, M. Moretti Sala, C. Mazzoli, Ruixing Liang, D. A. Bonn, W. N. Hardy, B. Keimer, G. A. Sawatzky, and D. G. Hawthorn "Distinct charge orders in the planes and chains of ortho-III ordered $YBa_2Cu_3O_{6+x}$ identified by resonant elastic x-ray scattering," Phys. Rev. Lett. **109**, 167001 (2012).

[4] A. J. Achkar, X. Mao, C. McMahon, *et al.*, "Impact of disorder on charge density wave order in $YBa_2Cu_3O_{6+\delta}$," to appear.

[5] B. Keimer, N. Belk, R. J. Birgeneau, A. Cassanho, C. Y. Chen, M. Greven, M. A. Kastner, A. Aharony, Y. Endoh, R. W. Erwin, and G. Shirane, "Magnetic excitations in pure, lightly doped, and weakly metallic La_2CuO_4," Phys. Rev. B **46**, 14034 (1992).

[6] In La_2CuO_4 there is long-range antiferromagnetic order below 325K, but this is entirely due to the inter-layer exchange interactions.

[7] S. Chakravarty, B. I. Halperin, and D. R. Nelson, "Low-temperature behavior of two-dimensional quantum antiferromagnets," Phys. Rev. Lett. **60**, 1057 (1988).

[8] A. M. Polyakov, "Interaction of goldstone particles in two dimensions. Applications to ferromagnets and massive Yang-Mills fields," Phys. Lett. B **59**, 79 (1975).

[9] S. Sachdev and E. Demler, "Competing orders in thermally fluctuating superconductors in two dimensions," Phys. Rev. B **69**, 144504 (2004).

[10] O. Zachar, S. A. Kivelson, and V. J. Emery, "Landau theory of stripe phases in cuprates and nickelates," Phys. Rev. B **57**, 1422 (1998).

[11] E. W. Carlson, V. J. Emery, S. A. Kivelson, D. Orgad, "Concepts in High Temperature Superconductivity," in *The Physics of Superconductors Vol II: Superconductivity in Nanostructures, High-T_c and Novel Superconductors, Organic Superconductors*, K. H. Bennemann and J. B. Ketterson Eds., Springer, Berlin (2004); arXiv:cond-mat/0206217 [cond-mat.supr-con].

[12] S. Sachdev, "Order and quantum phase transitions in the cuprate superconductors," Rev. Mod. Phys. **75**, 913 (2003).

[13] S. Sachdev and R. La Placa, "Bond order in two-dimensional metals with antiferromagnetic exchange interactions," Phys. Rev. Lett. **111**, 027202 (2013).

[14] S. A. Kivelson, E. Fradkin, and V. J. Emery, "Electronic liquid-crystal phases of a doped Mott insulator," Nature **393**, 550 (1998).

[15] M. A. Metlitski and S. Sachdev, "Quantum phase transitions of metals in two spatial dimensions: II. Spin density wave order," Phys. Rev. B **82**, 075128 (2010).

[16] K. B. Efetov, H. Meier, and C. Pépin, "Pseudogap state near a quantum critical point," Nature Physics **9**, 442 (2013).

[17] H. Meier, M. Einenkel, C. Pépin, and K. B. Efetov, "Effect of magnetic field on competition between superconductivity and charge order below the pseudogap state," Phys. Rev. B **88**, 020506(R) (2013)

[18] I. Affleck, Z. Zou, T. Hsu, and P. W. Anderson, "SU(2) gauge symmetry of the large-U limit of the Hubbard model," Phys. Rev. B **38**, 745 (1988);

[19] E. Dagotto, E. Fradkin, and A. Moreo, "SU(2) gauge invariance and order parameters in strongly coupled electronic systems," Phys. Rev. B **38**, 2926 (1988).

[20] P. A. Lee, N. Nagaosa, and X.-G. Wen, "Doping a Mott insulator: Physics of high-temperature superconductivity," Rev. Mod. Phys. **78**, 17 (2006).

[21] S.-C. Zhang, "A Unified Theory Based on SO(5) Symmetry of Superconductivity and Antiferromagnetism," Science **275**, 1089 (1997).

[22] D. R. Nelson and J. M. Kosterlitz, "Universal jump in the superfluid density of two-dimensional superfluids," Phys. Rev. Lett. **39**, 1201 (1977).

[23] Lu Li, Yayu Wang, Seiki Komiya, Shimpei Ono, Yoichi Ando, G. D. Gu, and N. P. Ong, "Diamagnetism and Cooper pairing above T_c in cuprates," Phys. Rev. B **81**, 054510 (2010).

[24] I. Kokanović, D. J. Hills, M. L. Sutherland, R. Liang, and J. R. Cooper, "Diamagnetism of $YBa_2Cu_3O_{6+x}$ crystals above T_c: Evidence for Gaussian fluctuations," Phys. Rev. B **88**, 060505(R) (2013).

[25] A. Larkin and A. Varlamov, *Theory of Fluctuations in Superconductors* (Clarendon, Oxford, U.K., 2005).

[26] V. Oganesyan, D. A. Huse, and S. L. Sondhi, "Theory of diamagnetic response of the vortex liquid phase of two-dimensional superconductors," Phys. Rev. B **73**, 094503 (2006).

[27] D. Podolsky, S. Raghu, and A. Vishwanath, "Nernst effect and diamagnetism in phase fluctuating superconductors," Phys. Rev. Lett. **99**, 117004 (2007).

[28] K. Sarkar, S. Banerjee, S. Mukerjee, and T. V. Ramakrishnan, "Fluctuation diamagnetism from a Ginzburg-Landau-like free energy functional for high-T_c superconductors," arXiv:1309.3776 [cond-mat.supr-con].

[29] S. Banerjee, Shizhong Zhang, and M. Randeria, "Quantum oscillations in a d-wave vortex liquid," Nature Communications **4**, Article number: 1700 (2013).

[30] J. E. Hoffman, E. W. Hudson, K. M. Lang, V. Madhavan, H. Eisaki, S. Uchida, and J. C. Davis, "A four unit cell periodic pattern of quasi-particle states surrounding vortex cores in $Bi_2Sr_2CaCu_2O_{8+\delta}$," Science **295**, 466 (2002).

[31] T. Wu, H. Mayaffre, S. Kramer, M. Horvatic, C. Berthier, P.L. Kuhns, A.P. Reyes, R. Liang, W.N. Hardy, D.A. Bonn, and M.-H. Julien, "Emergence of charge order from the vortex state of a high temperature superconductor," Nature Communications **4**, 2113 (2013).

[32] Y. Kohsaka, C. Taylor, K. Fujita, A. Schmidt, C. Lupien, T. Hanaguri, M. Azuma, M. Takano, H. Eisaki, H. Takagi, S. Uchida, and J. C. Davis, "An Intrinsic Bond-Centered Electronic Glass with Unidirectional Domains in Underdoped Cuprates," Science **315**, 1380 (2007).

[33] T. Wu, H. Mayaffre, S. Krämer, M. Horvatić, C. Berthier, W. N. Hardy, R. Liang, D.A. Bonn, and M.-H. Julien, "Magnetic-field-induced charge-stripe order in the high-temperature superconductor $YBa_2Cu_3O_y$," Nature **477**, 191 (2011).

[34] N. Doiron-Leyraud, C. Proust, D. LeBoeuf, J. Levallois, J.-B. Bonnemaison, Ruixing Liang, D. A. Bonn, W. N. Hardy, and L. Taillefer, "Quantum oscillations and the Fermi surface in an underdoped high-T_c superconductor," Nature **447**, 565 (2007).

[35] S. E. Sebastian, N. Harrison and G. G. Lonzarich, Rep. Prog. Phys. **75**, 102501 (2012).

[36] H. Karapetyan, Jing Xia, M. Hucker, G. D. Gu, J. M. Tranquada, M. M. Fejer, and

A. Kapitulnik, "Evidence of chiral order in the charge-ordered phase of $La_{1.875}Ba_{0.125}CuO_4$," arXiv:1308.4785 [cond-mat.str-el]

[37] T. Wu, H. Mayaffre, S. Krämer, M. Horvatić, C. Berthier, C. T. Lin, D. Haug, T. Loew, V. Hinkov, B. Keimer, and M.-H. Julien, "Magnetic field-enhanced spin freezing in $YBa_2Cu_3O_{6.45}$ at the verge of the competition between superconductivity and charge order," Phys. Rev. B **88**, 014511 (2013).

[38] S. Blanco-Canosa, A. Frano, T. Loew, Y. Lu, J. Porras, G. Ghiringhelli, M. Minola, C. Mazzoli, L. Braicovich, E. Schierle, E. Weschke, M. Le Tacon, and B. Keimer, "Momentum-Dependent Charge Correlations in $YBa_2Cu_3O_{6+\delta}$ Superconductors Probed by Resonant X-Ray Scattering: Evidence for Three Competing Phases," Phys. Rev. Lett. **110**, 187001 (2013).

[39] E. Brézin and J. Zinn-Justin, "Spontaneous breakdown of continuous symmetries near two dimensions," Phys. Rev. B **14**, 3110 (1976).

[40] D. Podolsky and S. Sachdev, "Spectral functions of the Higgs mode near two-dimensional quantum critical points," Phys. Rev. B **86**, 054508 (2012).